

Abstract

Implementing oxygen isotopes (H_2^{18}O , H_2^{16}O) in coupled climate models provides both an important test of the individual model's hydrological cycle, and a powerful tool to mechanistically explore past climate changes while producing results directly comparable to isotope proxy records. Here we describe the addition of oxygen isotopes in the University of Victoria Earth System Climate Model (UVic ESCM). Equilibrium simulations are performed for preindustrial and Last Glacial Maximum conditions. The oxygen isotope content in the model preindustrial climate is compared against observations for precipitation and seawater. The distribution of oxygen isotopes during the LGM is compared against available paleo-reconstructions.

1 Introduction

From ocean sediment cores to ice cores to speleothems to leaf wax, measurements of oxygen isotopes and the corresponding estimates of changes in temperature and the hydrologic cycle have permitted reconstructions of past climate variability. Isotope-enabled models have likewise figured prominently in questions concerning hydrologic cycling under modern and past climates. Since the pioneering implementation of stable water isotopes in the LMD atmospheric general circulation model (AGCM) by Joussaume et al. (1984), the modern distribution of stable water isotopes in the atmosphere is increasingly well captured in models (e.g., Hoffmann et al., 1998; Lee et al., 2007). Additionally, the comparison of modeled stable water isotope variability to isotope records from ice and sediment cores (e.g., Roche et al., 2004b; LeGrande et al., 2006) has undoubtedly advanced the understanding of past climate changes. Forward modeling of stable water isotopes, combined with model-data intercomparison, is likely to grow as an important contributor to understanding past climate changes.

Here we present the implementation of stable oxygen water isotopes (H_2^{18}O , H_2^{16}O) in the University of Victoria Earth System Climate Model (UVic ESCM). Oxygen isotope

GMDD

4, 2545–2576, 2011

Oxygen isotopes in the UVic ESCM

C. E. Brennan et al.

Title Page

Abstract

Introduction

Conclusions

References

Tables

Figures

◀

▶

◀

▶

Back

Close

Full Screen / Esc

Printer-friendly Version

Interactive Discussion



content is typically expressed as the ratio (R) $\text{H}_2^{18}\text{O}/\text{H}_2^{16}\text{O}$ or as $\delta^{18}\text{O}$ when referenced to the V-SMOW standard ($\delta^{18}\text{O} = (R/R_{\text{VSMOW}} - 1) \times 10^3$) in units of permil (‰). As an intermediate complexity model (due to it is 2-D, vertically integrated atmosphere), the UVic ESCM combines speed with a complete representation of ocean dynamics. Ultimately, the goal of modelling oxygen isotopes using the UVic ESCM is to investigate the distribution of isotopes in seawater under different climate conditions, with the objective of improving the interpretation of oxygen isotope records from ocean sediment cores.

2 Model description

2.1 UVic ESCM

The UVic ESCM version 2.9 is a fully coupled ocean-atmosphere-land surface-sea ice model without flux adjustments, fully described by Weaver et al. (2001) and Meissner et al. (2003). Horizontal resolution is uniformly 3.6° (longitude) by 1.8° (latitude) in all model subcomponents. The ocean general circulation model has 19 vertical levels. Ocean diffusivity in the horizontal is $k_h = 8 \times 10^2 \text{ m}^2 \text{ s}^{-1}$, and in the vertical varies from thermocline $k_v = 0.3 \times 10^{-4} \text{ m}^2 \text{ s}^{-1}$ to deep ocean $k_v = 1.3 \times 10^{-4} \text{ m}^2 \text{ s}^{-1}$ (after Bryan and Lewis, 1979). Ocean mixing caused by mesoscale eddies is parameterized via the Gent and McWilliams (1990) isopycnal diffusion scheme.

The atmosphere model consists of vertically-integrated energy and moisture balance equations, and is forced by seasonally-varying solar insolation and NCEP reanalysis winds (Kalnay et al., 1996). Atmospheric moisture transport is achieved through diffusion and advection by winds. More specifically, the moisture advection scheme applies a wind field calculated as the weighted average of the NCEP long term monthly mean winds (from atmospheric levels below 10 000 m) (Kalnay et al., 1996). The weighting of the NCEP winds decreases exponentially with height to account for the exponential decrease in atmospheric water vapor with height. Moisture diffusion coefficients vary with

Oxygen isotopes in the UVic ESCM

C. E. Brennan et al.

Title Page

Abstract

Introduction

Conclusions

References

Tables

Figures

◀

▶

◀

▶

Back

Close

Full Screen / Esc

Printer-friendly Version

Interactive Discussion



latitude and are held constant in time. Zonal diffusivity is essentially symmetric around the equator, and achieves peak values between 40 and 50° in both hemispheres. In contrast, meridional diffusivity is higher in the southern hemisphere, with peak values occurring between 40 and 50° S. Meridional (zonal) diffusivity ranges from 0.8 to $3.56 \times 10^6 \text{ m}^2 \text{ s}^{-1}$ (0.05 to $3.1 \times 10^7 \text{ m}^2 \text{ s}^{-1}$).

The land surface model employs a dynamic vegetation land surface scheme (MOSES/TRIFFID) using a one-layer soil moisture (leaky bucket) representation (Meissner et al., 2003), which runs off to one of thirty-two rivers according to which river catchment basin the gridcell is located within. Snow may accumulate as a single, height-varying layer in the land surface model, with snowmelt either replenishing soil moisture or contributing to river runoff when the soil is saturated.

The standard thermodynamic-dynamic sea ice model (Semtner, 1976; Hibler, 1979) employed here consists of sub-gridscale ice-covered and open-ocean categories, with a height-varying sea ice layer and elastic viscous plastic ice rheology (Hunke and Dukowicz, 1997). Snow falling on sea ice may accumulate as a single height-varying snow layer.

2.2 Implementation of oxygen isotopes

Moisture is modelled explicitly as humidity in the atmosphere model, soil moisture and lying snow in the land surface model, and ice and overlying snow in the sea ice model. The existing model moisture was assumed to consist of H_2^{16}O , and equivalent H_2^{18}O reservoirs were added. On land, H_2^{18}O is represented in soil moisture and in snow lying on the land surface. In the sea ice model, H_2^{18}O is represented in the ice layer and the overlying snow layer.

The rigid-lid ocean model employs a constant-volume assumption such that salt fluxes are substituted for moisture fluxes, necessitating the addition of both H_2^{18}O and H_2^{16}O as ocean tracers (as in Tindall et al., 2009). At the sea surface, variations in isotopic content result from evaporation, precipitation, sea ice growth and melt, and inputs

Oxygen isotopes in the UVic ESCM

C. E. Brennan et al.

Title Page

Abstract

Introduction

Conclusions

References

Tables

Figures

◀

▶

◀

▶

Back

Close

Full Screen / Esc

Printer-friendly Version

Interactive Discussion



of river runoff. Away from the sea surface, H_2^{18}O and H_2^{16}O are essentially passive tracers due to the absence of subsurface sources or sinks. While water-rock interaction occurring at the seafloor fractionates oxygen isotopes in seawater, with low (high) temperature interaction producing depleted (enriched) seawater (Walker and Lohmann, 1989), these rock-water isotope exchange processes are considered to be in isotopic balance on the time scales applicable to our model simulations (i.e. $< 10^5$ yr, contrasted with a shift of 1 ‰ every 10^8 yr described by Walker and Lohmann, 1989).

Following the implementation of stable water isotopes in other models (e.g., Hoffmann et al., 1998; Lee et al., 2007; Tindall et al., 2009), H_2^{18}O undergoes exchange across surface boundaries and fractionation during the appropriate phase changes, summarized in Table 1.

2.2.1 Condensation

Precipitation forms in the model when atmospheric relative humidity is above 85%. Precipitation occurs under Rayleigh (or open system) conditions, as rain or snow that forms in the model is immediately removed from the atmosphere without any exchange with ambient vapor (see Dansgaard (1964) and Joussaume and Jouzel (1993) for treatment of modelling precipitation in open versus closed systems). At temperatures above -20°C , all precipitation forms in thermal equilibrium with the atmospheric vapor and is enriched relative to the vapor by α , the equilibrium fractionation factor such that $R_{\text{precip}} = \alpha R_{\text{vapor}}$. As in Jouzel et al. (1987), we assume the isotopic vapor condenses to liquid at or above -10°C , and forms a solid otherwise. We apply the appropriate equilibrium fractionation factors from Majoube (1971a,b) for vapor-liquid and vapor-solid transitions (respectively). An additional kinetic fractionation is included at temperatures below -20°C to account for the effects of differential molecular diffusion of H_2^{18}O and H_2^{16}O through a supersaturated layer surrounding an ice crystal (described in Jouzel and Merlivat, 1984). After Schmidt et al. (2005), the supersaturation is parameterized as $S_{\text{ice}} = 1 - 0.004T$ (T is air temperature, $^\circ\text{C}$) (such that S_{ice} varies between

Title Page

Abstract

Introduction

Conclusions

References

Tables

Figures

◀

▶

◀

▶

Back

Close

Full Screen / Esc

Printer-friendly Version

Interactive Discussion



1 and the ratio of saturation vapor pressures of ice to water (see Jouzel et al., 1987). Fractionation effects during condensation are summarized in Table 1.

2.2.2 Evaporation

Fractionation during evaporation from the sea surface depends on the moisture and isotope gradients at the ocean-atmosphere interface, and takes into account both equilibrium effects (i.e. temperature-dependent) and kinetic effects (i.e. due to the differences in molecular diffusivity for H_2^{18}O and H_2^{16}O). The isotopic fluxes in evaporation are well described by the Craig-Gordon evaporation model (Craig and Gordon, 1965), which is based on a Langmuir resistance model. In the Craig-Gordon model, the evaporative flux of H_2^{16}O (E) is a simple function of the humidity gradient between the sea surface boundary (where relative humidity is equal to one) and aloft (characterized by relative humidity h). The evaporative flux driven by the humidity gradient is reduced by a resistivity parameter, ρ , such that $E = (1 - h)/\rho$. Likewise, the evaporative flux of H_2^{18}O (E_i) includes the additional assumption that the vapor at the sea surface boundary is in isotopic equilibrium with the seawater (therefore equal to $R_{\text{oc}}/\alpha_{\text{eq}}$), while the atmospheric water vapor aloft has isotopic content of R_v , giving $E_i = (R_{\text{oc}}\alpha_{\text{eq}}^{-1} - hR_v)/\rho_i$. As discussed in Gat (1996), the kinetic fractionation effects due to differential molecular diffusion in air for H_2^{18}O and H_2^{16}O are included in the resistivity coefficients. The resulting ratio of H_2^{18}O and H_2^{16}O in evaporation, or R_e , is simply equal to E_i/E , shown in Table 1.

When snow or ice sublimates, the entire sublimated layer is removed to the atmosphere, and no fractionation occurs. Likewise, transpiration by plants communicates unfractionated root water (i.e. soil moisture) to the atmosphere (Gat, 1996). Evaporation from bare soil is also returned to the atmosphere without fractionation. While evaporation from a soil column should include fractionation in theory, this process is neglected for the sake of simplicity (following most models). Since bare soil evaporation

Oxygen isotopes in the UVic ESCM

C. E. Brennan et al.

Title Page

Abstract

Introduction

Conclusions

References

Tables

Figures

◀

▶

◀

▶

Back

Close

Full Screen / Esc

Printer-friendly Version

Interactive Discussion



is small compared to the total evaporative flux, this simplification should have a minor effect. Fractionation processes during evaporation are summarized in Table 1.

2.2.3 Moisture transport over elevation

In an earlier version of the model, precipitation was not sufficiently depleted when atmospheric humidity was transported over grid cells containing higher land elevation (relative to the low elevation precipitation, as compared to both observations and AGCMs with multiple levels in the vertical). The likeliest explanation is that because the UVic model does not resolve atmospheric vertical convection, moisture transported to higher elevations would simply condense at colder temperatures from overly enriched vapor (as opposed to the depleted vapor aloft found in AGCMs, presumably via distillation from vertical air motion). To address this problem, we decreased the diffusion of H_2^{18}O by an elevation-dependent amount. The difference in atmospheric diffusivity between H_2^{18}O and H_2^{16}O is zero over ocean points, negligible over low elevation (most continental points), and important only over significant high elevation regions (Antarctica, Greenland, and the Himalayas), shown in Fig. 1.

3 Model evaluation

The model preindustrial climatology discussed here results from a 5,000 year simulation with constant boundary conditions of year 1800 orbital configuration and solar forcing, and $p\text{CO}_2$ of 283.87 ppm. The ocean model was initialized to 0.1 ‰, the atmosphere humidity to -10 ‰, and other water reservoirs to 0‰.

The UVic ESCM present day climatology has been fully described by Weaver et al. (2001). For reference, the model (preindustrial) surface air temperature and precipitation (both annual mean and seasonal variation, defined as DJF-JJA) are presented in Figs. 2 and 3. The differences between the model fields and the corresponding NCEP reanalysis fields are included to highlight model-data discrepancies, which could potentially shift the resulting distribution of isotopes.

Oxygen isotopes in the UVic ESCM

C. E. Brennan et al.

Title Page

Abstract

Introduction

Conclusions

References

Tables

Figures

◀

▶

◀

▶

Back

Close

Full Screen / Esc

Printer-friendly Version

Interactive Discussion



The annual average temperature in the model closely resembles that of NCEP (Fig. 2). Eastern Antarctica, northeastern North America, and northeastern Asia are warmer in the model relative to observations, with the largest discrepancy in Eastern Antarctica. The seasonal difference in temperature (DJF-JJA) is slightly damped in the model relative to NCEP, especially over Northern Hemisphere continents and Eastern Antarctica.

With respect to precipitation, the model reproduces the global pattern of observed annual precipitation, and the model global mean precipitation rate is close to the observed value (respectively, 2.89 and 2.74 mm day⁻¹). The highest observed precipitation rates in the annual mean are underestimated by the model, such as in Amazonia (Fig. 3), a feature common across models. Differences in seasonality in precipitation (DJF-JJA) between the model and NCEP are most pronounced over southern and eastern Asia, eastern North America, Central America, and central Africa.

Below we focus on the modeled distribution of oxygen isotopes in moisture fluxes and seawater, and compare the modeled isotope patterns to observations.

3.1 Isotopes in precipitation

Dansgaard (1964) described a set of isotope effects relating the oxygen isotopic content in precipitation ($\delta^{18}O_{\text{precip}}$) to factors including precipitation amount, latitude, surface air temperature, distance from the coast, and altitude. These observed relationships are all produced by the total amount of moisture lost from an air mass (known as rain-out) as it travels away from its moisture source (Rozanski et al., 1993). The degree to which the UVic model can capture these observed patterns in $\delta^{18}O_{\text{precip}}$ is a function of the accuracy of the modeled temperature, evaporation, and precipitation fields, as well as the representation of moisture transport. As shown in Fig. 4 (top panel), model annual zonal mean moisture flux quantities (here, precipitation, evaporation, and E-P, the difference between evaporation and precipitation) all fall within one standard deviation of NCEP annual mean values at all latitudes.

Oxygen isotopes in the UVic ESCM

C. E. Brennan et al.

Title Page

Abstract

Introduction

Conclusions

References

Tables

Figures

◀

▶

◀

▶

Back

Close

Full Screen / Esc

Printer-friendly Version

Interactive Discussion



Oxygen isotopes in the UVic ESCM

C. E. Brennan et al.

[Title Page](#)[Abstract](#)[Introduction](#)[Conclusions](#)[References](#)[Tables](#)[Figures](#)[◀](#)[▶](#)[◀](#)[▶](#)[Back](#)[Close](#)[Full Screen / Esc](#)[Printer-friendly Version](#)[Interactive Discussion](#)

Observations of isotopes in precipitation have been collected at several hundred stations since the 1960's, forming the Global Network of Isotopes in Precipitation (GNIP) (IAEA, 2006). While the model zonal mean isotopic content in precipitation falls within the range of the GNIP long term mean $\delta^{18}\text{O}$ values at most latitudes (with the exception of the latitude band -30 to -70°S) (Fig. 4, right panel), the zonal mean $\delta^{18}\text{O}_{\text{precip}}$ is more enriched than GNIP observations on average. The model $\delta^{18}\text{O}_{\text{precip}}$ globally averaged value of -7.5‰ is within the range of values reported from AGCMs (-6 to -7.5‰ , see Table 3).

Figure 5 maps both the modeled mean annual $\delta^{18}\text{O}_{\text{precip}}$ and the long-term mean values at each GNIP station supplemented with Antarctic surface snow isotopic observations from Masson-Delmotte et al. (2008). Consistent with the latitude effect, $\delta^{18}\text{O}_{\text{precip}}$ decreases poleward in the model, reaching a minimum value of -47.1‰ in central Antarctica (in the Northern Hemisphere, a minimum of -26.2‰ is achieved in northern Greenland). A local enrichment ($+4.4\text{‰}$) occurs in southeast Asia on the lee side of the Himalaya. This feature is not found in the observations, and likely results from the elevation-dependent modification of H_2^{18}O diffusivity described in Sect. 2.5. While the model $\delta^{18}\text{O}_{\text{precip}}$ exhibits close to observed latitudinal patterns, regional discrepancies between modeled and observed are evident. For example, the regions of northern North America, northern Europe and southern South America are too enriched in the model. Otherwise, the model is generally consistent with observations throughout Asia (not including the aforementioned enrichment east of the Himalayas), Australia, Africa, and Antarctica. For mean annual temperatures below 15°C , the spatial relationship between temperature and $\delta^{18}\text{O}_{\text{precip}}$ is very similar in slope between model (sampled at GNIP station locations) and GNIP data (slope of 0.50 in the model vs. 0.49 in the data, with r^2 values of 0.88 and 0.81, respectively), shown in Fig. 6.

3.2 Isotopes in seawater

The distribution of oxygen isotopes at the ocean model surface reflects the isotopic fluxes occurring during evaporation from the sea surface, precipitation, additions of river runoff, and sea ice melt and brine production, in addition to the effects of transport and mixing of water masses. The model $\delta^{18}\text{O}$ at the sea surface (top 50 m) is presented with the interpolated observations (averaged over the top 50 m) (LeGrande and Schmidt, 2006) based on the GISS seawater O18 dataset (Schmidt et al., 1999) in Fig. 7. The oxygen isotope composition of seawater ($\delta^{18}\text{O}_{\text{sw}}$) in the model displays the same broad features found in the observations. Surface water is more depleted at high latitudes than in low latitudes. Net evaporative regions (where $P-E < 0$) contain more positive $\delta^{18}\text{O}_{\text{sw}}$ values. The Atlantic, for example, contains more enriched $\delta^{18}\text{O}_{\text{sw}}$ values than the Pacific. These observed large-scale patterns suggest the model produces a reasonable first-order distribution of moisture fluxes. A model-data discrepancy, however, is apparent in the absolute range of surface $\delta^{18}\text{O}_{\text{sw}}$ values, narrower in the model than in observations. This reduced variability in surface $\delta^{18}\text{O}_{\text{sw}}$ may result from the treatment of moisture transport and condensation in the atmospheric model.

3.2.1 Salinity- $\delta^{18}\text{O}$ relationships

Both seawater $\delta^{18}\text{O}$ and salinity are shifted in the same direction by processes occurring at the ocean surface (with the noted exception of sea ice growth and melt e.g., Strain and Tan, 1993), resulting in a linear relationship between the two quantities. For example, evaporation (precipitation) typically increases (decreases) both salinity and $\delta^{18}\text{O}_{\text{sw}}$. We compare the slope of the best fit line for the salinity- $\delta^{18}\text{O}$ data sampled from the model to that sampled from the same region in the observations.

We define surface waters as the top 400 m, and in the model the top four ocean levels, which corresponds to a depth of 380 m, within the salinity range of 28 to 38. Tropical surface waters (between 20°N and 20°S) have very similar model and observed salinity- $\delta^{18}\text{O}_{\text{sw}}$ relationships (Fig. 8). In the tropical Atlantic, we find a model slope (in

GMDD

4, 2545–2576, 2011

Oxygen isotopes in the UVic ESCM

C. E. Brennan et al.

Title Page

Abstract

Introduction

Conclusions

References

Tables

Figures

◀

▶

◀

▶

Back

Close

Full Screen / Esc

Printer-friendly Version

Interactive Discussion



salinity- $\delta^{18}\text{O}$ space) of 0.19 ($r^2 = 0.86$) and an observed slope of 0.18 ($r^2 = 0.70$). In the tropical Pacific, we find salinity- $\delta^{18}\text{O}$ slopes of 0.23 ($r^2 = 0.98$) in the model and 0.24 ($r^2 = 0.88$) in the observations. Model-data similarity decreases slightly in tropical Indian Ocean surface waters which have a salinity- $\delta^{18}\text{O}$ slope of 0.16 ($r^2 = 0.74$) in the model and 0.24 ($r^2 = 0.75$) in the data. In comparison, the extratropical surface water salinity- $\delta^{18}\text{O}$ relationship is weaker in the model than in the observations. The model slope of 0.32 ($r^2 = 0.88$) is significantly less than the observed slope of 0.57 ($r^2 = 0.83$). Similarly, the surface waters of the global ocean have a slope of 0.32 ($r^2 = 0.89$) in the model, which is less than the slope of 0.55 ($r^2 = 0.82$) observed in the data (Fig. 8).

Intermediate waters (400 to 2500 m) have a global mean salinity and $\delta^{18}\text{O}$ of 34.7 psu and 0.10 ‰ in the model, indistinguishable from the GISS seawater O18 dataset values of 34.9 psu and 0.10 ‰ for intermediate water ($n > 5400$). The salinity- $\delta^{18}\text{O}_{\text{sw}}$ spatial relationship in global intermediate waters is slightly reduced in the model than in the data (slope of 0.23 ($r^2 = 0.72$) vs. 0.39 ($r^2 = 0.87$), respectively). In the model, as in observations, deep water (>2500 m) is more saline and more enriched in H_2^{18}O in the North Atlantic than in the other ocean basins. While observations reveal the global deep ocean to be on average 0.3 to 0.45 ‰ more negative than deep water in the North Atlantic, the difference in the model is less dramatic, approximately 0.1 ‰.

4 Last glacial maximum equilibrium simulation

A 5,000 year simulation was performed using constant boundary conditions for the Last Glacial Maximum (LGM), including an orbital configuration corresponding to 21 kyr BP, atmospheric pCO_2 of 189.65 ppm, and increased elevations where ice had accumulated on land (following the Peltier (1994) ICE4G reconstruction). The model was initialized using a previous LGM simulation such that the ocean and climate physical parameters were already at quasi-equilibrium values. In order to initialize the water isotope reservoirs, recent estimates of the difference between LGM and present day values were considered. By applying a pore water diffusion model to a deep western

Oxygen isotopes in the UVic ESCM

C. E. Brennan et al.

Title Page

Abstract

Introduction

Conclusions

References

Tables

Figures

◀

▶

◀

▶

Back

Close

Full Screen / Esc

Printer-friendly Version

Interactive Discussion



Pacific sediment core, Schrag et al. (1996) estimated a 1.0 ± 0.25 ‰ LGM seawater enrichment, relative to present day. Duplessy et al. (2002) considered the full range of LGM sea level estimates (120–140 m), and with the same methods (i.e., Schrag et al., 1996; Adkins and Schrag, 2001) concluded that the LGM ocean was enriched relative to present day by 0.95–1.08‰. Duplessy et al. (2002) further assessed all other robust methods for estimating the LGM seawater isotopic shift, and determined a best estimate of 1.05 ± 0.20 ‰. We therefore initialized the LGM ocean to 1.1‰ above the pre-industrial seawater initial value of 0.1‰. Ice on land was set to -30 ‰, atmospheric water vapor to -10 ‰, and other water reservoirs (sea ice, snow lying on land and sea ice, and soil moisture) to 0‰.

4.1 LGM climatology

The modeled LGM climatological patterns (e.g. surface air temperatures and ocean temperatures) are very similar to the LGM simulation described by Weaver et al. (2001). As shown in Fig. 9, the LGM global mean temperature is cooler by 4.08 °C, and global mean precipitation is decreased by 0.19 mm day⁻¹, relative to the preindustrial (PI). Precipitation is slightly enhanced only in a narrow mid-latitude band in each hemisphere. Climatological mean values for the LGM and PI simulations as well as the LGM-PI differences are presented in Table 2.

As in previous LGM simulations in the UVic model, relative to the preindustrial the maximum meridional overturning streamfunction is reduced (14.4 Sv in the LGM compared to preindustrial 21.7 Sv), sea ice cover is expanded (2.5×10^{13} m² during LGM compared to a preindustrial annual mean of 2.2×10^{13} m²), and sea surface temperature is decreased (the largest decrease, >8 °C, is found in the northeast Atlantic, while the mean tropical SST change is -2.4 °C) except in the polar oceans where expanded sea ice cover decreases heat loss to the atmosphere (not shown, see Figs. 37–39 in Weaver et al., 2001).

GMDD

4, 2545–2576, 2011

Oxygen isotopes in the UVic ESCM

C. E. Brennan et al.

Title Page

Abstract

Introduction

Conclusions

References

Tables

Figures

◀

▶

◀

▶

Back

Close

Full Screen / Esc

Printer-friendly Version

Interactive Discussion



4.1.1 Isotopes in LGM precipitation

Atmospheric water vapor and precipitation are slightly more enriched at low latitudes in the LGM simulation compared to preindustrial (Fig. 9). A similar slight increase in low latitude $\delta^{18}\text{O}_{\text{precip}}$ is found in other models (e.g., LMDZ-iso AGCM results shown in Figs. 12–13 in Risi et al., 2010). The model is able to capture the LGM depletion in Northern Hemisphere high latitudes, but the magnitude of the depletion is smaller over northern North America than in the LMDZ-iso AGCM. For example, the model maximum decrease in annual mean $\delta^{18}\text{O}_{\text{precip}}$ is 10.6‰, while in LMDZ-iso LGM precipitation falling in the Hudson Bay region is depleted by more than 15 to 25‰ relative to present day (depending on which LGM SST forcing is applied). The model LGM-PI depletion in the Southern Hemisphere high latitudes is rather weak (less than 2.5‰), and whereas the LMDZ-iso AGCM only produces an enrichment near the Antarctic coast (see Fig. 13 in Risi et al., 2010), the model simulates an enrichment over inland Eastern Antarctica.

We can compare model LGM $\delta^{18}\text{O}_{\text{precip}}$ to the $\delta^{18}\text{O}$ values measured from ice cores and cave deposits formed during the LGM (Table 2). Risi et al. (2010) compiled estimates from the most recently available ice core, cave deposit, and aquifer records spanning the LGM (their Table 2). The compilation includes the isotopic content in ice measured in fifteen ice cores from high-latitude (Greenland and Antarctica), mid-latitude (Tibet), and low-latitude (South America) ice cores, and the isotopic content determined at seven mid- and low-latitude cave and aquifer sites. The estimate of LGM $\delta^{18}\text{O}_{\text{precip}}$ at each site may be characterized by various types of uncertainty, including dating uncertainty as noted by Risi et al. (2010).

The model LGM-PI difference in mean annual $\delta^{18}\text{O}_{\text{precip}}$ indicates that the simulated LGM may not be as depleted relative to preindustrial as observations suggest (Fig. 10). The model-data discrepancy is largest in northwestern Greenland and eastern Antarctica, and small at sites in Southern Africa, South-Eastern Asia, Southern Greenland, England and along the east coast of South America.

GMDD

4, 2545–2576, 2011

Oxygen isotopes in the UVic ESCM

C. E. Brennan et al.

Title Page

Abstract

Introduction

Conclusions

References

Tables

Figures

◀

▶

◀

▶

Back

Close

Full Screen / Esc

Printer-friendly Version

Interactive Discussion



5 Summary and conclusions

Stable water isotopes have been implemented in a range of atmosphere, ocean, and coupled models to date (see Table 3). Of these, few are fully coupled atmosphere-ocean models, and fewer still are Earth system models of intermediate complexity (or EMICs). The isotope-enabled UVic ESCM may fill a unique role in that it is an intermediate complexity model with a full ocean GCM (as opposed to the EMIC CLIMBER-2 with a zonally-averaged 3-basin ocean model), and the atmosphere and ocean models are fully-coupled for all fluxes (heat, moisture, oxygen isotopes, etc.).

When undertaking the implementation of H_2^{18}O and H_2^{16}O in the UVic model, we were initially skeptical as to whether the final distribution of $\delta^{18}\text{O}$ would prove sufficiently realistic, given the simplified atmospheric sub-component of the model, and especially the model formulation of condensation (i.e. precipitation forms when relative humidity exceeds 85 %). Isotopic fluxes resulting from dynamical, small-scale processes that are neglected in the model can simply not be captured. Nevertheless, as noted below, our analysis indicates that the UVic model succeeds in capturing the broad pattern and magnitude of $\delta^{18}\text{O}$ composition in mean annual precipitation and seawater.

We have performed long (5 kyr) equilibrium model simulations under preindustrial and LGM boundary conditions and compared the resulting isotope fields to available data. In our evaluation of the model isotope distribution, we find that the model reproduces the large-scale patterns in precipitation and seawater isotopic content. At the regional scale, the model is reasonably consistent with preindustrial $\delta^{18}\text{O}_{\text{precip}}$ observations throughout Australia, Africa, South America, and across Asia (with the exception of the locally enriched area east of the Himalayas). The Antarctic region contains the maximum depletion in $\delta^{18}\text{O}_{\text{precip}}$ both in the model and in observations, although precipitation in the model is not as depleted as observations from the Antarctic Surface Snow Dataset (Masson-Delmotte et al., 2008) suggest. Likewise, northern North America (Canada) is too enriched in the model relative to observations.

GMDD

4, 2545–2576, 2011

Oxygen isotopes in the UVic ESCM

C. E. Brennan et al.

Title Page

Abstract

Introduction

Conclusions

References

Tables

Figures

◀

▶

◀

▶

Back

Close

Full Screen / Esc

Printer-friendly Version

Interactive Discussion



Oxygen isotopes in the UVic ESCM

C. E. Brennan et al.

Title Page

Abstract

Introduction

Conclusions

References

Tables

Figures

◀

▶

◀

▶

Back

Close

Full Screen / Esc

Printer-friendly Version

Interactive Discussion



Under preindustrial forcing, the model reproduces the observed large-scale sea surface isotopic patterns, including enrichment in evaporative regions and depletion at high latitudes, but the model is not as depleted as the observations in northern high-latitude seawater. This shortcoming is reflected in the model salinity- $\delta^{18}\text{O}$ relationship in surface waters, which while similar to the observations in the tropics, is significantly weaker in extratropical surface waters. Model and observations are highly similar for salinity and $\delta^{18}\text{O}$ values in intermediate and deep waters.

Given this result, we suggest that the isotope-enabled UVic ESCM may be best utilized in performing simulations requiring integrations over long time scales, in combination with determining oxygen isotopic anomalies (between simulated climate states). For example, one useful application may involve investigating variability in seawater isotopic content under distinct climate states. Finally, the model may be well suited to improving the interpretation of oxygen isotope records from ocean sediment cores. The implementation of oxygen isotopes in the UVic ESCM adds new functionality to this intermediate-complexity model, allowing exploration of the potential processes determining the distribution of $\delta^{18}\text{O}$ for a given climate.

Acknowledgements. We are grateful to several modelers who previously implemented stable water isotopes into ocean and atmosphere models for their helpful suggestions. We thank Claude Hillaire-Marcel for his comments assisting in the comparison of model results to available ocean data. This work has been generously supported by the Canadian Foundation for Climate and Atmospheric Sciences, the Natural Sciences and Engineering Research Council of Canada (NSERC) CREATE program, a NSERC Discovery Grant, and the Australian Research Council Future Fellowships.

References

- Adkins, J. F. and Schrag, D. P.: Pore fluid constraints on deep ocean temperature and salinity during the last glacial maximum, *Geophys. Res. Lett.*, 28, 771–774, 2001. 2556
- Bryan, K. and Lewis, L.: A water mass model of the world ocean, *J. Geophys. Res.*, 84, 311–337, 1979. 2547

Oxygen isotopes in the UVic ESCM

C. E. Brennan et al.

Title Page

Abstract

Introduction

Conclusions

References

Tables

Figures

◀

▶

◀

▶

Back

Close

Full Screen / Esc

Printer-friendly Version

Interactive Discussion



- Craig, H. and Gordon, L. I.: Deuterium and oxygen-18 variations in the ocean and marine atmosphere, in: *Stable Isotopes in Oceanographic Studies and Paleo-Temperatures*, edited by: Tongiorgi, E., 9–130, Pisa: Lab. Geol. Nucl., 1965. 2550, 2564
- Dansgaard, W.: Stable isotopes in precipitation, *Tellus*, 16, 436–468, 1964. 2549, 2552
- 5 Delaygue, G., Jouzel, J., and Dutay, J.-C.: Oxygen 18salinity relationship simulated by an oceanic general circulation model, *Earth Planet. Sci. Lett.*, 178, 113–123, 2000. 2566
- Duplessy, J.-C., Labeyrie, L., and Waelbroeck, C.: Constraints on the ocean oxygen isotopic enrichment between the Last Glacial Maximum and the Holocene: Paleooceanographic implications, *Quat. Sci. Rev.*, 21, 315–330, 2002. 2556, 2565, 2576
- 10 Gat, J. R.: Oxygen and hydrogen isotopes in the hydrologic cycle, *Annu. Rev. Earth Planet. Sci.*, 24, 225–262, 1996. 2550, 2564
- Gent, P. R. and McWilliams, J. C.: Isopycnal mixing in ocean circulation models, *J. Phys. Ocean.*, 20, 150–155, 1990. 2547
- Hibler, W. D.: A dynamic thermodynamic sea ice model, *J. Phys. Oceanogr.*, 9, 815–846, 1979. 2548
- 15 Hoffmann, G., Werner, M. and Heimann, M.: Water isotope module of the ECHAM atmospheric general circulation model: a study on timescales from days to several years, *J. Geophys. Res.*, 103, 16871–16896, 1998. 2546, 2549, 2566
- Hunke, E. C. and Kukowicz J. K.: An elastic-viscous-plastic model for sea ice dynamics, *J. Phys. Oceanogr.*, 27, 1849–1867, 1997. 2548
- 20 IAEA/WMO, Global Network of Isotopes in Precipitation, The GNIP Database, available at: <http://www.iaea.org/water>, 2006. 2553, 2570, 2571
- Joussaume, S., Jouzel, J., and Sadoury, R.: A general circulation model of water isotope cycles in the atmosphere, *Nature*, 311, 24–29, 1984. 2546, 2566
- 25 Joussaume, S. and Jouzel, J.: Paleoclimatic tracers: an investigation using an atmospheric general circulation model under ice age conditions 2. Water isotopes, *J. Geophys. Res.*, 98, 2807–2830, 1993. 2549
- Jouzel, J. and Merlivat, L.: Deuterium and O-18 in precipitation: Modeling of the isotopic effects during snow formation, *J. Geophys. Res.*, 89, 1749–1757, 1984. 2549, 2564
- 30 Jouzel, J., Russell, G. L., Suozzo, R. J., Koster, R. D., White, J. W. C., and Broecker, W. S.: Simulations of the HDO and H₂¹⁸O atmospheric cycles using the NASA GISS general circulation model: the seasonal cycle for present-day conditions, *J. Geophys. Res.*, 92, 14739–14760, 1987. 2549, 2550, 2564, 2566

Oxygen isotopes in the UVic ESCM

C. E. Brennan et al.

Title Page

Abstract

Introduction

Conclusions

References

Tables

Figures

◀

▶

◀

▶

Back

Close

Full Screen / Esc

Printer-friendly Version

Interactive Discussion



- Kalnay E., Kanamitsu, M., Kistler, R., Collins, W., Deaven, D., Gandin, L., Iredell, M., Saha, S., White, G., Woollen, J., Zhu, Y., Chelliah, M., Ebisuzaki, W., Higgins, W., Janowiak, J., Mo, K. C., Ropelewski, C., Wang, J., Leetma, A., Reynolds, R., Jenne, R., and Joseph, D. The NCEP/NCAR 40-year reanalysis project, *B. Am. Meteorol. Soc.* 77, 437–471, 1996. 2547, 2565, 2570
- Lee, J.-E., Fung, I., DePaolo, D. J., and Henning, C. C.: Analysis of the global distribution of water isotopes using the NCAR atmospheric general circulation model, *J. Geophys. Res.*, 112, D16306, doi:10.1029/2006JD007657, 2007. 2546, 2549, 2566, 2570
- LeGrande, A. N. and Schmidt, G. A.: Global gridded data set of the oxygen isotopic composition in seawater, *Geophys. Res. Lett.*, 33, L12604, doi:10.1029/2006GL026011, 2006. 2554, 2573
- LeGrande, A. N., Schmidt, G. A., Shindell, D. T., Field, C. V., Miller, R. L., Koch, D. M., Faluvegi, G., and Hoffmann, G.: Consistent simulations of multiple proxy responses to an abrupt climate change event, *Proceedings of the Natl. Proc. Acad. Sci. USA*, 103, 837–842, 2006. 2546
- Majoube, M.: Fractionnement en oxygene 18 et en deuterium entre l'eau et sa vapeur, *J. Chem. Phys.*, 10, 1423–1436, 1971a. 2549, 2564
- Majoube, M.: Fractionnement en oxygene 18 entre la glace et la vapeur d'eau, *J. Chem. Phys.*, 68, 625–636, 1971b. 2549, 2564
- Marsh, R., Smith, M. P. L. M., Rohling, E. J., Lunt, D. J., Lenton, T. M., Williamson, M. S., and Yool, A.: Modelling ocean circulation, climate and oxygen isotopes in the ocean over the last 120 000 years, *Clim. Past Discuss.*, 2, 657–709, doi:10.5194/cpd-2-657-2006, 2006. 2566
- Masson-Delmotte, V., Hou, S., Ekaykin, A., Jouzel, J., Aristarain, A., Bernardo, R. T., Bromwich, D., Cattani, O., Delmotte, M., Falourd, S., Frezzotti, M., Gallée, H., Genoni, L., Isaksson, E., Landais, A., Helsen, M. M., Hoffmann, G., Lopez, J., Morgan, V., Motoyama, H., Noone, D., Oerter, H., Petit, J. R., Royer, A., Uemura, R., Schmidt, G. A., Schlosser, E., Simões, J. C., Steig, E. J., Stenni, B., Stievenard, M., van den Broeke, M. R., van de Wal, R. S. W., van de Berg, W. J., Vimeux, F., and White, J. W. C.: A review of Antarctic surface snow isotopic composition: Observations, atmospheric circulation and isotopic modelling, *J. Climate*, 21, 3359–3387, 2008. 2553, 2558, 2571
- Mathieu, R., Pollard, D., Cole, J. E., White, J. W. C., Webb, R. S., and Thompson, S. L.: Simulation of stable water isotope variations by the GENESIS GCM for modern conditions, *J. Geophys. Res.*, 107, 4037, doi:10.1029/2001JD900255, 2002. 2566

Oxygen isotopes in the UVic ESCM

C. E. Brennan et al.

Title Page

Abstract

Introduction

Conclusions

References

Tables

Figures

◀

▶

◀

▶

Back

Close

Full Screen / Esc

Printer-friendly Version

Interactive Discussion



Meissner, K. J., Weaver, A. J., Matthews H. D., and Cox, P. M.: The role of land surface dynamics in glacial inception: a study with the UVic Earth System Model, *Clim. Dynam.*, 21, 515–537, 2003. 2547, 2548

Noone, D. and Simmonds, I.: Associations between $\delta^{18}\text{O}$ of water and climate parameters in a simulation of atmospheric circulation for 1979–95, *J. Climate*, 15, 3150–3169, 2002. 2566

Noone, D. and Sturm, C.: Comprehensive dynamical models of global and regional water isotope distributions, in: *Isoscapes: Understanding Movement, Pattern, and Process on Earth Through Isotope Mapping*, edited by: West, J. B., Bowen, G. J., Dawson, T. E., and Tu, K. P., Springer, New York, 195–219, 2010. 2566

O’Neil, J. R.: Hydrogen and oxygen isotope fractionation between ice and water, *J. Phys. Chem.*, 72, 3683–3684, 1968. 2564

Peltier, W. R.: Ice age paleotopography, *Science*, 265, 195–201, 1994. 2555

Risi, C., Bony, S., Vimeux, F., and Jouzel, J.: Water-stable isotopes in the LMDZ4 general circulation model: Model evaluation for present-day and past climates and applications to climatic interpretations of tropical isotopic records, *J. Geophys. Res.*, 115, D12118, doi:10.1029/2009JD013255, 2010. 2557, 2565, 2566, 2576

Roche, D., Paillard, D., Ganopolski, A., and Hoffmann, G.: Oceanic oxygen-18 at the present day and LGM: equilibrium simulations with a coupled climate model of intermediate complexity, *Earth Planet. Sci. Lett.*, 218, 317–330, 2004. 2566

Roche, D., Paillard, D., and Cortijo, E.: Constraints on the duration and freshwater release of Heinrich event 4 through isotope modelling, *Nature*, 432, 379–382, 2004. 2546

Rozanski, K., Araguas-Araguas, L., and Gonfiantini, R.: Isotopic patterns in modern global precipitation, in *Change in Continental Isotopic Records*, *Geophys. Monogr. Ser.*, 78, 1–36, 1993. 2552

Schmidt, G. A.: Oxygen-18 variations in a global ocean model, *Geophys. Res. Lett.*, 25, 1201–1204, 1998. 2566

Schmidt, G. A., Bigg, G. R., and Rohling, E. J.: Global Seawater Oxygen-18 Database – v1.20, available at: <http://data.giss.nasa.gov/o18data>, 1999. 2554, 2574

Schmidt, G. A., A. N. LeGrande, and G. Hoffmann, Water isotope expressions of intrinsic and forced variability in a coupled ocean-atmosphere model, *J. Geophys. Res.*, 112, D10103, doi:10.1029/2006JD007781, 2007. 2566

Schmidt, G. A., Hoffmann, G., Shindell, D. T., and Hu, Y.: Modeling atmospheric stable water isotopes and the potential for constraining cloud processes and stratosphere-troposphere

**Oxygen isotopes in
the UVic ESCM**

C. E. Brennan et al.

[Title Page](#)[Abstract](#)[Introduction](#)[Conclusions](#)[References](#)[Tables](#)[Figures](#)[I◀](#)[▶I](#)[◀](#)[▶](#)[Back](#)[Close](#)[Full Screen / Esc](#)[Printer-friendly Version](#)[Interactive Discussion](#)

- water exchange, *J. Geophys. Res.*, 110, D21314, doi:10.1029/2005JD005790, 2005. 2549
- Schrag, D. P., Hampt, G., and Murray, D. W.: Pore fluid constraints on the temperature and oxygen isotopic composition of the glacial ocean, *Science*, 272, 1930–1932, 1996. 2556
- 5 Semtner, A. J.: A model for the thermodynamic growth of sea ice in numerical investigations of climate, *J. Phys. Oceanogr.*, 6, 379–389, 1976. 2548
- Strain, P. M. and Tan, F. C.: Seasonal evolution of oxygen isotope-salinity relationships in high-latitude surface waters, *J. of Geophys. Res.*, 98, 14589–14598, 2003. 2554
- Tindall, J. C., Valdes, P. J., and Sime, L. C.: Stable water isotopes in HadCM3: isotopic signature of El Nino-Southern Oscillation and the tropical amount effect, *J. Geophys. Res.*, 114, D04111, doi:10.1029/2008JD010825, 2009. 2548, 2549, 2566
- 10 Walker, J. C. G. and Lohmann, K. C.: Why the oxygen isotopic composition of sea water changes with time, *Geophys. Res. Lett.*, 16, 323–326, 1989. 2549
- Weaver, A. J., Eby, M., Wiebe, E. C., Bitz, C. M., Duffy, P. B., Ewen, T. L., Fanning, A. F., Holland, M. M., MacFadyen, A., Matthews, H. D., Meissner, K. J., Saenko, O., Schmittner, A., Wang, H., and Yoshimori, M.: The UVic Earth System Climate Model: Model description, climatology, and applications to past, present and future climates, *Atmos.-Ocean*, 39, 361–428, 2001. 2547, 2551, 2556
- 15 Yoshimura, K., Oki, T., Ohte, N., and Kanae, S.: A quantitative analysis of short-term ^{18}O variability with a Rayleigh-type isotope circulation model, *J. Geophys. Res.*, 108, 4647, doi:10.1029/2003JD003477, 2003. 2566
- Yoshimura, K., Kanamitsu, M., Noone, D., and Oki, T.: Historical isotope simulation using Reanalysis atmospheric data, *J. Geophys. Res.*, 113, D19108, doi:10.1029/2008JD010074, 2008. 2566
- 20 Zhou, J., Poulsen, C. J., Pollard, D., and White, T. S.: Simulation of modern and middle Cretaceous marine $\delta^{18}\text{O}$ with an ocean-atmosphere general circulation model, *Paleoceanography*, 23, PA3223, doi:10.1029/2008PA001596, 2008. 2566, 2570
- 25

Table 1: Oxygen isotope fractionation during surface exchanges and phase changes.

Process	Fractionation	
Condensation, vapor-liquid ($T \geq -10^\circ\text{C}$)	$R_p = \alpha_{\text{eq}} R_v$	$\ln \alpha_{\text{eq}} = \frac{1.137 \times 10^3}{T^2} - \frac{0.4156}{T} - 2.0667 \times 10^{-3}$ Majoube (1971a)
Condensation, vapor-ice ($T < -10^\circ\text{C}$)	$R_p = \alpha_{\text{eq}} R_v$	$\ln \alpha_{\text{eq}} = \frac{11.839}{T} - 28.224 \times 10^{-3}$ Majoube (1971b)
Condensation, vapor-ice ($T < -20^\circ\text{C}$)	$R_p = \alpha_{\text{eq}} \alpha_{\text{kin}} R_v$	$\ln \alpha_{\text{eq}} = \frac{11.839}{T} - 28.224 \times 10^{-3}$ Majoube (1971b)
		$\alpha_{\text{kin}} = \frac{S}{\alpha_{\text{eq}} \times \frac{\rho_i}{\rho} \times (S-1) + 1}$ Jouzel and Merlivat (1984)
		$S = 1 - 0.00047$ Jouzel et al. (1987)
Evaporation from sea surface	$R_e = \frac{\alpha_{\text{eq}}^{-1} R_{\text{oc}} - h R_v}{(1-h)(\frac{\rho_i}{\rho})}$	$\ln \alpha_{\text{eq}} = \frac{1.137 \times 10^3}{T^2} - \frac{0.4156}{T} - 2.0667 \times 10^{-3}$ Majoube (1971a)
		$\frac{\rho_i}{\rho} - 1 = \theta \cdot n \cdot C_D$ Gat (1996)
Evaporation from soils	$R_e = R_s$	
Freezing (sea ice growth), liquid-ice	$R_i = \alpha_{\text{eq}} R_{\text{oc}}$	$\alpha_{\text{eq}} = 1.003$ O'Neil (1968)
Sublimation, solid-vapor	$R_v = R_i$	
Transpiration, liquid-vapor	$R_e = R_s$	

R = mass ratio $\text{H}_2^{18}\text{O}/\text{H}_2^{16}\text{O}$ for precipitation (p), atmospheric vapor (v), ice (i), evaporation (e), seawater (oc), and soil moisture (s); α = fractionation factor, with α_{eq} and α_{kin} the equilibrium and kinetic fractionation factors (respectively); S = supersaturation parameter; T = temperature (in K for α_{eq} expressions, $^\circ\text{C}$ for S expression); D , $D_1 = \text{H}_2^{16}\text{O}$, H_2^{18}O diffusivities; h = relative humidity; ρ_i/ρ = ratio of effective resistances for H_2^{18}O and H_2^{16}O (in the Craig and Gordon, 1965 linear-resistance type model for evaporation of isotopic species); following Gat (1996), evaporation under open-water conditions is represented in the selection of constants $\theta = 0.5$ and $n = 0.5$, while $C_D = 28.5 \text{‰}$.

Title Page

Abstract

Introduction

Conclusions

References

Tables

Figures

◀

▶

◀

▶

Back

Close

Full Screen / Esc

Printer-friendly Version

Interactive Discussion



Oxygen isotopes in the UVic ESCM

C. E. Brennan et al.

Table 2: Climatological and isotopic annual mean values from the preindustrial (PI) and Last Glacial Maximum (LGM) model equilibrium simulations, the difference between LGM and PI (LGM-PI), and available reference data for comparison. Low and mid-latitudes refer to 0–30° N, S and 30–60°N, respectively. Where reference time period not specified, value refers to PI. For LGM-PI data references, see Table 2 in Risi et al. (2010) and Table 2 in Duplessy et al. (2002).

	PI	LGM	LGM-PI	Reference value
Surface air temp., global	13.26 °C	9.18 °C	−4.08 °C	
Surface ocean temp., global	17.86 °C	15.57 °C	−2.29 °C	
Precipitation, global	2.89 mm day ^{−1}	2.70 mm day ^{−1}	−0.19 mm day ^{−1}	2.74 mm day ^{−1} (Kalnay et al., 1996)
$\delta^{18}\text{O}_{\text{precip.}}$, global	−7.5 ‰	−7.4 ‰	0.1 ‰	
$\delta^{18}\text{O}_{\text{precip.}}$, marine	−4.2 ‰	−3.9 ‰	−0.3 ‰	
Greenland $\delta^{18}\text{O}_{\text{precip}}$				
GRIP ice core	−16.7 ‰	−19.5 ‰	−2.8 ‰	LGM-PI: −7 ‰
Camp Century ice core	−19.7 ‰	−22.9 ‰	−3.2 ‰	LGM-PI: −12.9 ‰
Dye 3 ice core	−4.0 ‰	−7.5 ‰	−3.5 ‰	LGM-PI: −5.5 ‰
Renland ice core	−10.5 ‰	−13.6 ‰	−3.0 ‰	LGM-PI: −5 ‰
NGRIP ice core	−19.5 ‰	−20.7 ‰	−1.2 ‰	LGM-PI: −8 ‰
Mid-latitude $\delta^{18}\text{O}_{\text{precip}}$				
England	−3.8 ‰	−3.8 ‰	0.0 ‰	LGM-PI: −1.2 ‰
Gullya ice core	−4.6 ‰	−3.6 ‰	+1.0 ‰	LGM-PI: −5.4 ‰
Dunde ice core	−6.7 ‰	−6.2 ‰	+0.5 ‰	LGM-PI: −2 ‰
Sanbao and Hulu caves	1.2 ‰	2.1 ‰	+0.9 ‰	LGM-PI: +1.5 ‰
Low-latitude $\delta^{18}\text{O}_{\text{precip}}$				
Stampriet aquifer	−1.4 ‰	−0.1 ‰	+1.3 ‰	LGM-PI: +1.5 ‰
Huascaran ice core	−3.2 ‰	−1.9 ‰	+1.3 ‰	LGM-PI: −6.3 ‰
Sajama ice core	−3.0 ‰	−1.7 ‰	+1.2 ‰	LGM-PI: −5.4 ‰
Illimani ice core	−1.1 ‰	0.3 ‰	+1.4 ‰	LGM-PI: −6 ‰
Botuvera cave	−1.3 ‰	−0.1 ‰	+1.2 ‰	LGM-PI: −1.5 ‰
Santana cave	−1.5 ‰	−0.3 ‰	+1.2 ‰	LGM-PI: −1.5 ‰
Rio Grande do Norte cave	−1.7 ‰	−0.5 ‰	+1.2 ‰	LGM-PI: −0.5 ‰
Salar de Uyuni	−2.4 ‰	−1.3 ‰	+1.2 ‰	LGM-PI: −4 ‰
Antarctica $\delta^{18}\text{O}_{\text{precip}}$				
Vostok	−36.5 ‰	−32.9 ‰	+3.6 ‰	LGM-PI: −3 ‰ to −5 ‰
Byrd	−21.4 ‰	−23.0 ‰	−1.6 ‰	LGM-PI: −8 ‰
Dome C	−28.8 ‰	−27.2 ‰	+1.6 ‰	LGM-PI: −5.4 ‰
Dome B	−35.6 ‰	−32.0 ‰	+3.7 ‰	LGM-PI: −5 ‰
Taylor Dome	−36.3 ‰	−35.1 ‰	+1.2 ‰	LGM-PI: −3 ‰

Title Page

Abstract

Introduction

Conclusions

References

Tables

Figures

◀

▶

◀

▶

Back

Close

Full Screen / Esc

Printer-friendly Version

Interactive Discussion



Table 3: Global general circulation and intermediate complexity models with stable water isotopes. If it was reported, the global mean $\delta^{18}\text{O}_{\text{precip}}$ value is given (NA if isotopes are not explicitly modeled in atmospheric precipitation).

Models	Reference	Global mean $\delta^{18}\text{O}_{\text{precip}}$
Atmospheric GCMS		
ECHAM	Hoffmann et al. (1998)	(N. Atl. vapor -12‰)
GENESIS	Mathieu et al. (2002)	
GISS	Jouzel et al. (1987)	
ICM	Yoshimura et al. (2003)	
LMD	Joussaume et al. (1984)	
LMDZ4	Risi et al. (2010)	-7.56‰
MUGCM	Noone and Simmonds (2002)	
NCAR CAM2	Lee et al. (2007)	
NCAR CAM3	Noone and Sturm (2010)	
ECPC GSM	Yoshimura et al. (2008)	-6.5 to -7.0‰
Ocean GCMs		
CCM3	Delaygue et al. (2000)	NA
GISS	Schmidt (1998)	NA
AOGCMs		
GENESIS-MOM	Zhou et al. (2008)	-7.1‰
GISS ModelE	Schmidt et al. (2007)	-6.0‰ (vapor -13.0‰)
HadCM3	Tindall et al. (2009)	
EMICs		
CLIMBER-2	Roche et al. (2004a)	NA
GENIE-1	Marsh et al. (2006)	NA
UVic ESCM	This work	-7.5‰

LMDZ4 global $\delta^{18}\text{O}$ mean value is for AMIP simulation 1979 annual mean Risi et al., 2010. Yoshimura et al., 2008 provide a range of monthly global mean $\delta^{18}\text{O}_{\text{precip}}$ for ECPC GSM.

Oxygen isotopes in the UVic ESCM

C. E. Brennan et al.

[Title Page](#)

[Abstract](#) [Introduction](#)

[Conclusions](#) [References](#)

[Tables](#) [Figures](#)

[◀](#) [▶](#)

[◀](#) [▶](#)

[Back](#) [Close](#)

[Full Screen / Esc](#)

[Printer-friendly Version](#)

[Interactive Discussion](#)



Oxygen isotopes in the UVic ESCM

C. E. Brennan et al.

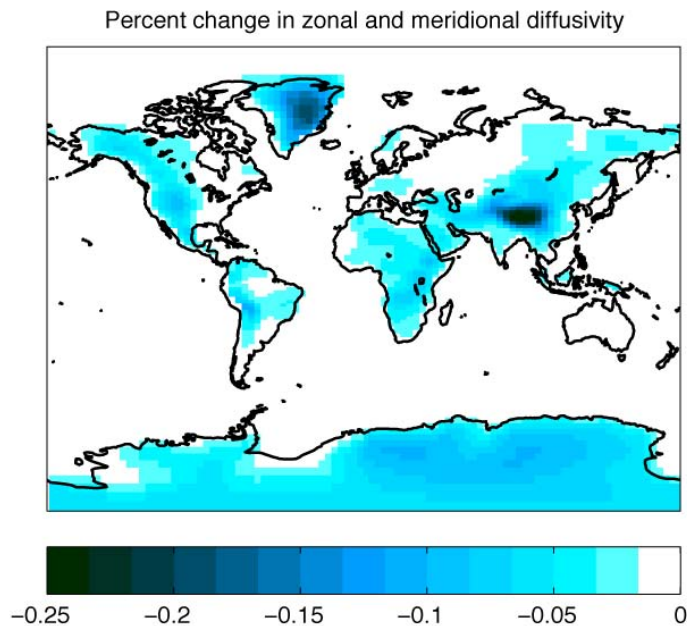


Fig. 1: Model atmospheric water vapor diffusivity adjustment. Percent change in zonal and meridional diffusivity for H_2^{18}O relative to H_2^{16}O (maximum reduction is 0.25 %).

[Title Page](#)[Abstract](#)[Introduction](#)[Conclusions](#)[References](#)[Tables](#)[Figures](#)[⏪](#)[⏩](#)[◀](#)[▶](#)[Back](#)[Close](#)[Full Screen / Esc](#)[Printer-friendly Version](#)[Interactive Discussion](#)

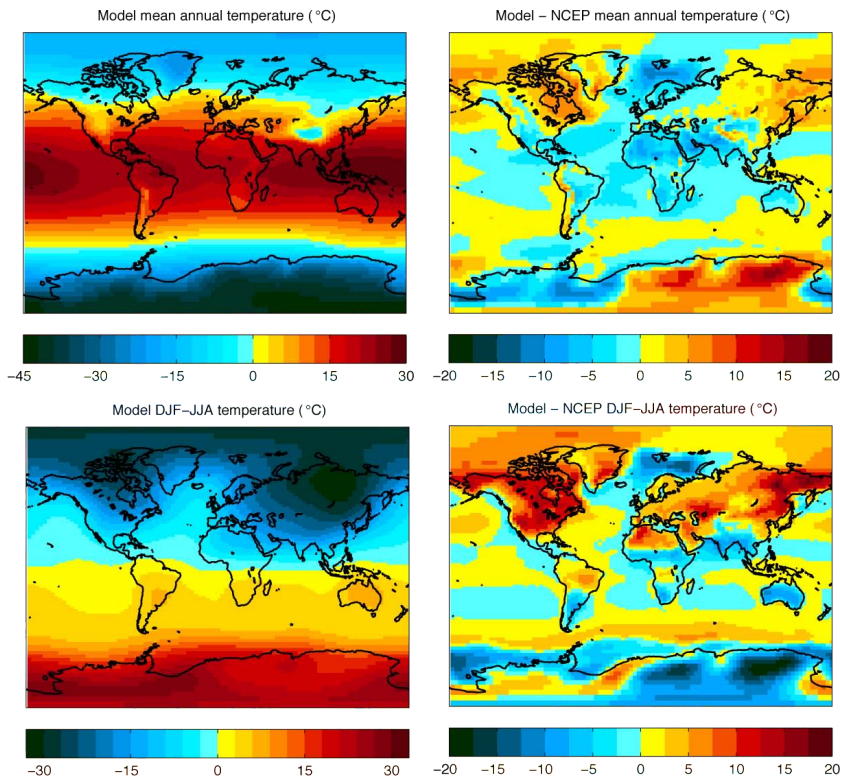


Fig. 2: Model surface air temperature climatology. Temperature ($^{\circ}\text{C}$) in the annual mean UVic model pre-industrial simulation (top left), the difference between the model and NCEP reanalysis annual means (top right), seasonal variation in the UVic model (DJF-JJA) (bottom left), and the difference in seasonality between the model and NCEP reanalysis DJF-JJA.

Oxygen isotopes in the UVic ESCM

C. E. Brennan et al.

[Title Page](#)

[Abstract](#) [Introduction](#)

[Conclusions](#) [References](#)

[Tables](#) [Figures](#)

[◀](#) [▶](#)

[◀](#) [▶](#)

[Back](#) [Close](#)

[Full Screen / Esc](#)

[Printer-friendly Version](#)

[Interactive Discussion](#)



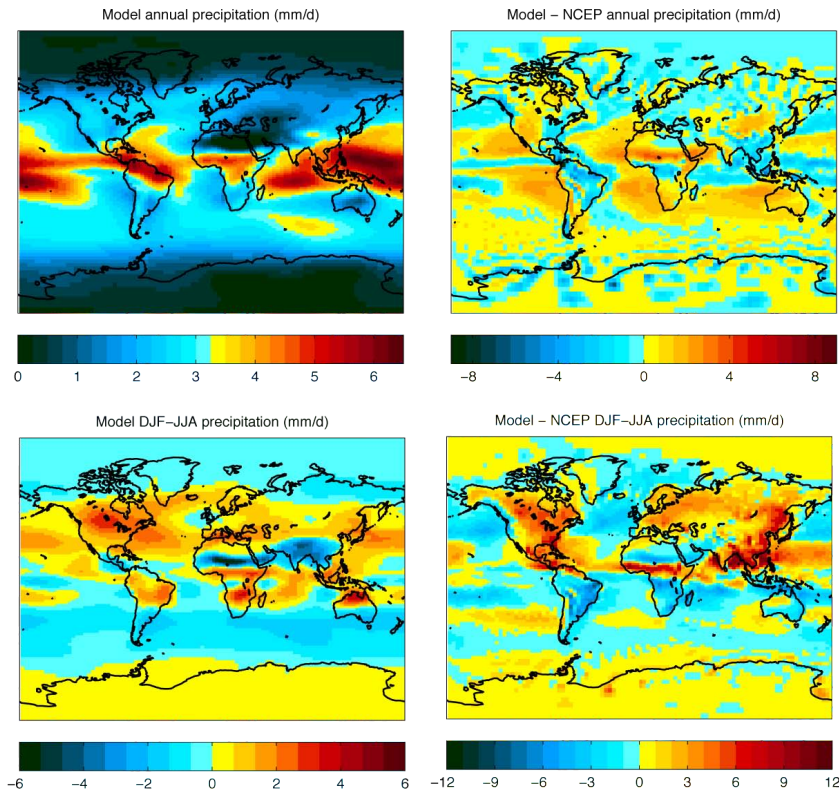


Fig. 3: Model precipitation climatology. Precipitation (mm day^{-1}) in the annual mean UVic model pre-industrial simulation (top left), the difference between the model and NCEP reanalysis annual means (top right), seasonal variation in the UVic model (DJF-JJA) (bottom left), and the difference in seasonality between the model and NCEP reanalysis DJF-JJA.

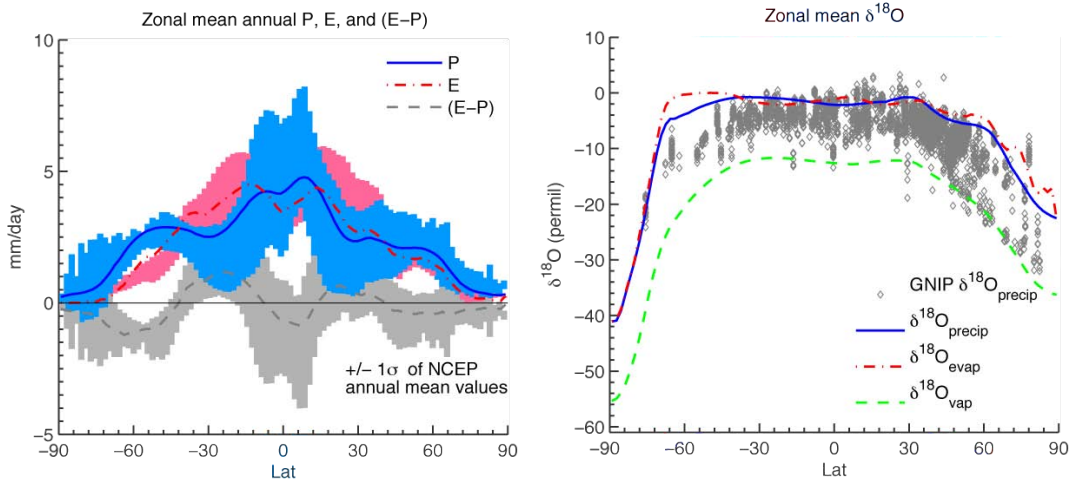


Fig. 4: Zonal mean fluxes of moisture and isotopes. Zonal annual mean precipitation (solid blue line), evaporation (red dash-dot line), and E-P (dark gray dashed line) in the UVic model, superimposed upon the range of the NCEP zonal annual mean values $\pm 1\sigma$ observed in precipitation (blue bars), evaporation as calculated from NCEP latent heat fluxes (pink bars), and E-P (light gray bars) (left), and zonal annual mean $\delta^{18}\text{O}$ in precipitation (blue solid line), evaporation (red dash-dot) and atmospheric water vapor (green dash) (right) in the model, superimposed upon all available annual mean precipitation $\delta^{18}\text{O}$ observations in GNIP data (gray diamonds), separated into $1/4^\circ$ latitude bins. NCEP reanalysis data are from Kalnay et al. (1996); GNIP $\delta^{18}\text{O}$ data are provided by IAEA (2006). Figure based on Fig. 12 in Lee et al. (2007) and Fig. 1 in Zhou et al. (2008).

Oxygen isotopes in the UVic ESCM

C. E. Brennan et al.

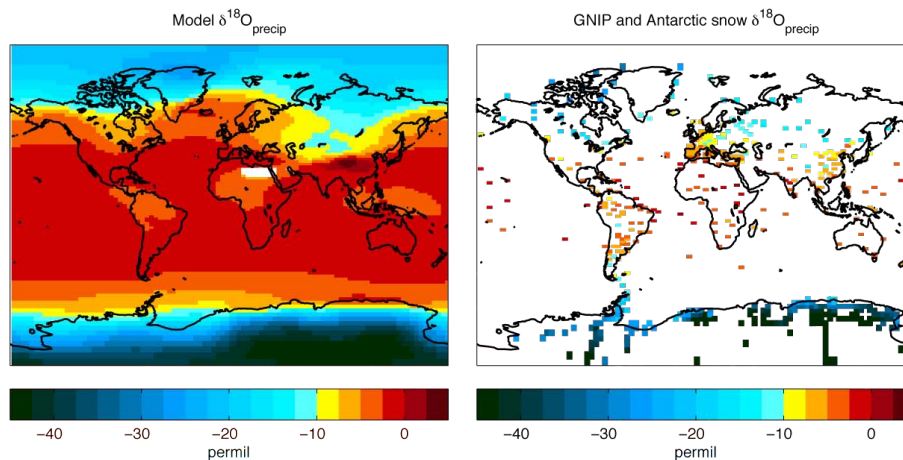


Fig. 5: $\delta^{18}\text{O}$ in precipitation. Annual average $\delta^{18}\text{O}$ in present-day precipitation for the UVic model (left) and observations from the Global Network of Isotopes in Precipitation (IAEA, 2006) and Antarctic surface snow (Masson-Delmotte et al., 2008) datasets (right). Observational values are plotted at a slightly larger size than the actual gridcell (130 %) for improved visualization.

[Title Page](#)[Abstract](#)[Introduction](#)[Conclusions](#)[References](#)[Tables](#)[Figures](#)[⏪](#)[⏩](#)[◀](#)[▶](#)[Back](#)[Close](#)[Full Screen / Esc](#)[Printer-friendly Version](#)[Interactive Discussion](#)

Oxygen isotopes in the UVic ESCM

C. E. Brennan et al.

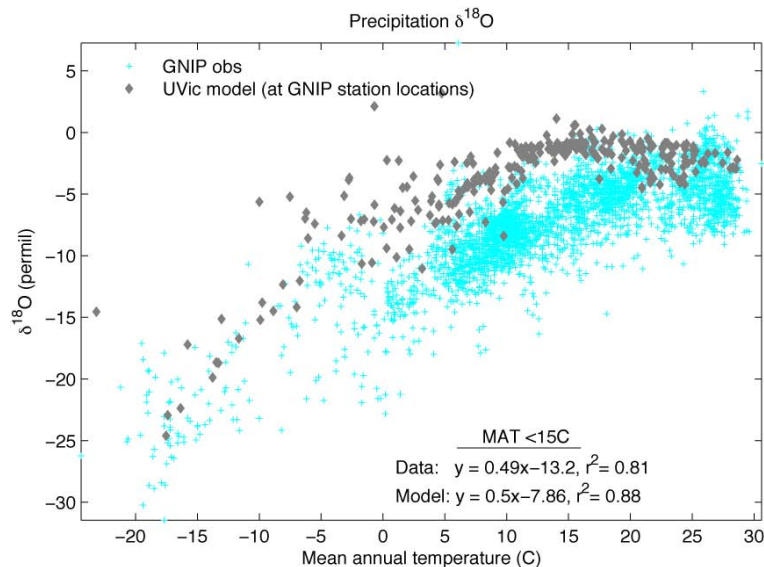


Fig. 6: Temperature – $\delta^{18}\text{O}$ spatial relationship. Mean annual temperature and $\delta^{18}\text{O}$ in precipitation are plotted for observations at GNIP stations (blue crosses) and the UVic model at GNIP station locations (gray diamonds). The linear fit for GNIP and model values with mean annual temperature less than 15°C is indicated.

[Title Page](#)[Abstract](#)[Introduction](#)[Conclusions](#)[References](#)[Tables](#)[Figures](#)[◀](#)[▶](#)[◀](#)[▶](#)[Back](#)[Close](#)[Full Screen / Esc](#)[Printer-friendly Version](#)[Interactive Discussion](#)

Oxygen isotopes in the UVic ESCM

C. E. Brennan et al.

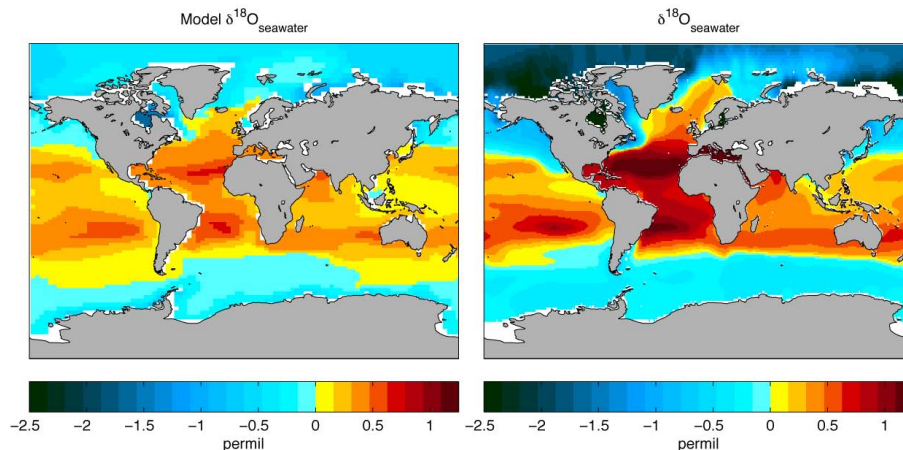


Fig. 7: Sea surface $\delta^{18}\text{O}$. Surface seawater $\delta^{18}\text{O}$ in the UVic model (annual mean of surface ocean model level (depth 50 m)) (left), and the gridded $\delta^{18}\text{O}$ seawater dataset (LeGrande and Schmidt, 2006) (averaged over the top 50 m) (right).

[Title Page](#)[Abstract](#)[Introduction](#)[Conclusions](#)[References](#)[Tables](#)[Figures](#)[⏪](#)[⏩](#)[◀](#)[▶](#)[Back](#)[Close](#)[Full Screen / Esc](#)[Printer-friendly Version](#)[Interactive Discussion](#)

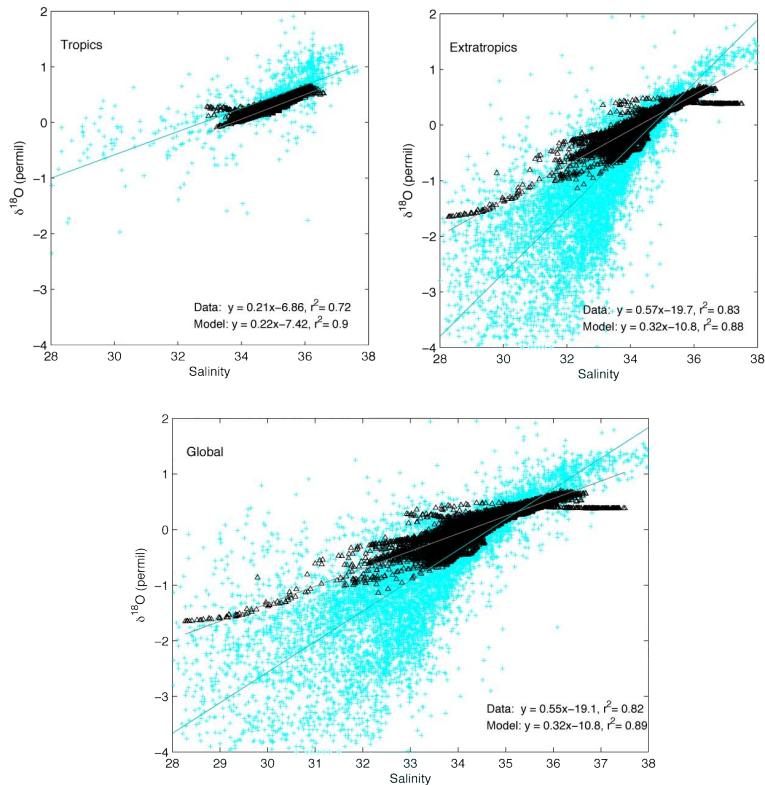


Fig. 8: Salinity- $\delta^{18}\text{O}$ spatial relationships in seawater. Surface water salinity- $\delta^{18}\text{O}$ relationships found in the model preindustrial annual mean (black diamonds) and the Seawater O18 dataset (Schmidt et al., 1999) (blue crosses) in the tropics (20°S – 20°N) (top left), extratropics ($>20^\circ\text{N}$ and S) (top right), and in the global surface waters (bottom). The linear fit to the observations (blue line) and model values (gray line) is indicated in the lower right.

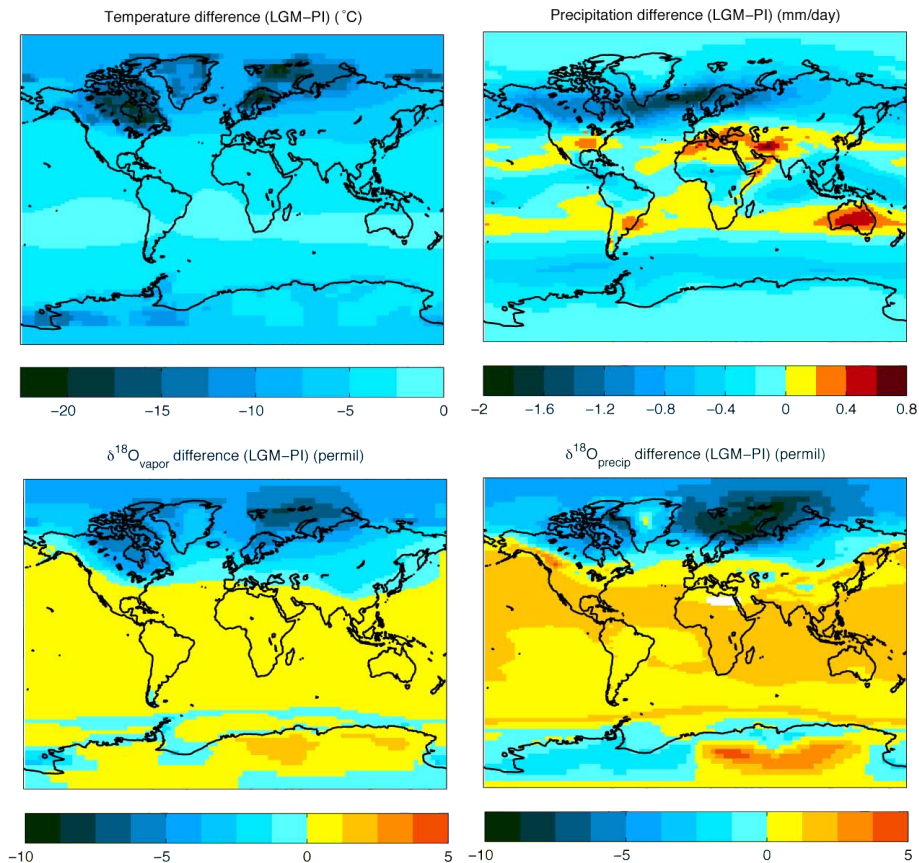


Fig. 9: Model LGM-PI climatological and isotopic differences. Annual mean difference between LGM and PI for surface air temperature (top left), precipitation (top right), $\delta^{18}\text{O}$ in atmospheric water vapor (bottom left), and $\delta^{18}\text{O}$ in precipitation (bottom right).

Oxygen isotopes in the UVic ESCM

C. E. Brennan et al.

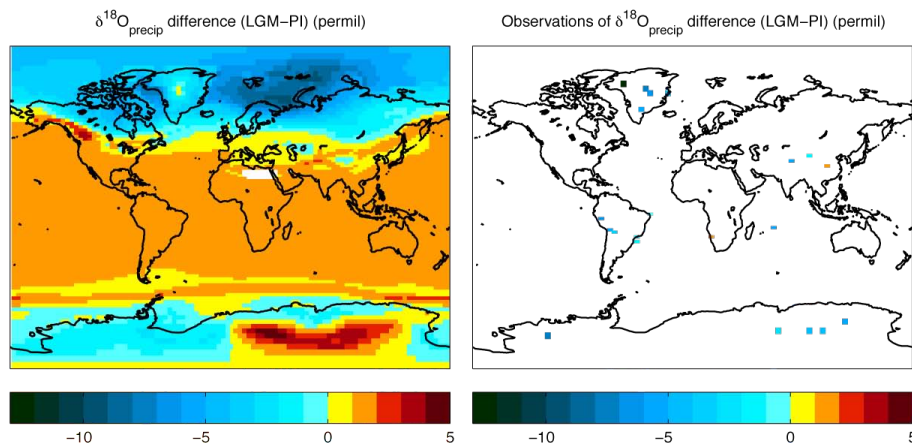


Fig. 10: Model and observed LGM-PI $\delta^{18}\text{O}_{\text{precip}}$ differences. Annual mean difference between LGM and PI for $\delta^{18}\text{O}$ in precipitation in the model (left) and the data (right). Observational values are plotted at a slightly larger size than the actual gridcell (130 %) for improved visualization. LGM-PI data is summarized in Table 2. Complete references are provided in Table 2 in Duplessy et al. (2002) and Table 2 in Risi et al. (2010).

Title Page

Abstract

Introduction

Conclusions

References

Tables

Figures

⏪

⏩

◀

▶

Back

Close

Full Screen / Esc

Printer-friendly Version

Interactive Discussion

